

Quadrupole-Induced Resonant-Particle Transport in a Pure Electron Plasma

E. P. Gilson* and J. Fajans†

Department of Physics, University of California, Berkeley, California 94720

(Received 12 August 2002; revised manuscript received 28 October 2002; published 8 January 2003)

Small transverse magnetic quadrupole fields sharply degrade the confinement of non-neutral plasmas held in Malmberg-Penning traps. For example, a quadrupole magnetic field of only 0.02 G/cm doubles the diffusion rate in a trap with a 100 G axial magnetic field. Larger quadrupole fields noticeably change the shape of the plasma. The transport is greatest at an orbital resonance. These results cast doubt on plans to use magnetic quadrupole neutral atom traps to confine antihydrogen atoms created in double-well positron/antiproton Malmberg-Penning traps.

DOI: 10.1103/PhysRevLett.90.015001

PACS numbers: 52.27.Jt, 52.25.Fi

An axially invariant, transverse, quadrupole magnetic field can dramatically change the shape and transport rates of non-neutral plasmas confined in Malmberg-Penning traps. Experiments show that these effects depend on whether the plasma is above or below a resonance between the plasma rotation frequency and the end-to-end bounce frequency of the plasma particles. The transport near resonance is strong, even for the relatively modest quadrupole fields used in this experiment.

The effects of magnetic field asymmetries are relevant to the general study of resonant particle transport in Malmberg-Penning traps [1–5] and in tandem mirror machines [6–10]. This work, however, was motivated by the cold, trapped antihydrogen ($\bar{\text{H}}$) generation teams, ATHENA [11] and ATRAP [12], who hope to test the *CPT* invariance of the standard model. Antihydrogen can be generated by mixing trapped positrons and antiprotons [13]; to capture $\bar{\text{H}}$ atoms, however, the neutral antihydrogen atoms must be confined in the same physical location as the positrons and antiprotons. We show here that the magnetic quadrupole neutral atom traps proposed to confine the antihydrogen will likely destroy the confinement of the positrons and antiprotons in the Malmberg-Penning traps.

Malmberg-Penning traps consist of a series of three or more collimated, cylindrical, conducting rings immersed in a strong axial magnetic field, B_z , as shown in Fig. 1. Voltages applied to the end rings provide axial confinement, and the axial magnetic field provides radial confinement. The traps can confine electrons, positrons, or antiprotons; for electrons, the plasma source is a tungsten filament. Momentarily grounding the first ring loads the electrons into the trap. Grounding the last ring dumps the electrons out of the trap. All Malmberg-Penning traps employ an axial magnetic field B_z ; here we also employ a transverse, axially invariant, quadrupole magnetic field. The total magnetic field (Fig. 2) is

$$\mathbf{B} = B_z \hat{\mathbf{z}} + \beta_1(x\hat{\mathbf{x}} - y\hat{\mathbf{y}}) + \beta_2(y\hat{\mathbf{x}} + x\hat{\mathbf{y}}), \quad (1)$$

where β_1 and β_2 correspond to the fields from two sets of

orthogonal coils. The total quadrupole field strength is $\beta = \sqrt{\beta_1^2 + \beta_2^2}$. In this experiment, B_z ranges from 40 to 1500 G and $\beta \leq 1.0$ G/cm. Although these quadrupole fields are weak compared to the axial field, they produce clear shape changes and strong transport.

The ten rings of radius $r_w = 1.905$ cm in our trap allow us to vary the plasma length L from 5 to 28 cm. For typical parameters such as $kT = 1$ eV, $L = 28$ cm, $B_z = 100$ G, and plasma density $n = 10^7$ cm $^{-3}$, the time for a typical electron to traverse the trap once is $t_T = L/v_z = 0.7$ μ s and the $\mathbf{E} \times \mathbf{B}$ plasma rotation frequency about the trap axis (caused by the plasma's self-electric field) is $\omega = 3 \times 10^6$ rad s $^{-1}$.

As the quadrupole field has twofold symmetry, there exists a resonance condition,

$$\omega t_T = \frac{N\pi}{2}, \quad (2)$$

such that an electron rotates about the trap axis by an integer multiple N times $\pi/2$ during the time it takes to travel the length of the trap. If ω is independent of radius, an on-resonance electron travels ever outwards or inwards following the magnetic field lines as it bounces from end to end. The direction taken by the electron is set by its initial angle in the xy plane relative to the quadrupole angle $\theta_o = \frac{1}{2} \tan^{-1}(\beta_1/\beta_2)$. We define above ($>$) and below ($<$) resonance by the conditions $\omega t_T \gtrless \pi/2$. Off-resonance electrons will travel radially one way, and then

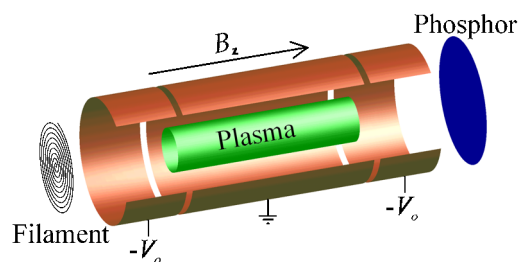


FIG. 1 (color online). A cutaway drawing of a simplified Malmberg-Penning trap showing the confinement rings, the filament, the plasma, and the phosphor screen.

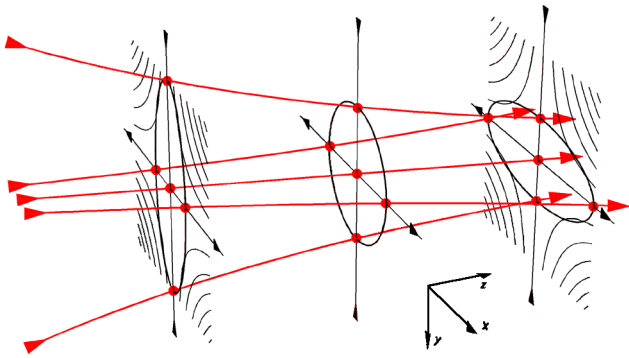


FIG. 2 (color online). Magnetic field lines for the transverse quadrupole field and for the total magnetic field. A flux tube that is circular at some arbitrary center $z = 0$ is elliptical for $z \neq 0$.

the other, as their phase slips relative to an on-resonance electron. Resonances exist for all the odd integers N , but higher order resonances are less dramatic.

As the plasma electrons' axial velocities are thermally distributed, some electrons are above resonance while others are below resonance. A good indicator of the average electron's behavior is whether or not an electron with the thermal velocity $v_{th} = \sqrt{kT/m}$ is above or below resonance. Henceforth we will use v_{th} to define t_T and speak of the plasma itself being above or below resonance.

When the plasma is below resonance, $\omega t_T \ll 1$, the electrons bounce many times before they rotate significantly. Hence, they follow the field lines in Fig. 2 and the plasma has the shape of a magnetic flux tube: circular in the center and elliptical on each end, but with the end ellipses rotated by 90° with respect to one another. Above resonance, when $\omega t_T \gg 1$, the radial excursions engendered by the quadrupole field average out and the plasma is cylindrical.

The ellipticity ϵ of the plasma [14], defined as the rms height of the plasma cross section divided by the rms width, can be determined by measuring the image charges induced on the trap wall. One of the confinement rings is divided azimuthally into four 90° sectors. The ellipticity $\epsilon - 1$ is proportional [15] to the signal $(V_1 + V_3) - (V_2 + V_4)$, where the V_i are the voltages induced on the four wall sectors. By manipulating the voltages on the ten rings in the trap, the plasma can be moved such that the sectored ring surrounds any desired axial position of the plasma. For below-resonance plasmas (see Fig. 3), $\epsilon - 1$ is zero at the plasma center and is equal and opposite at the two plasma ends $\pm z_o$ (corresponding to the ellipticity having rotated by 90°). As expected, $\epsilon - 1$ is proportional to β . Measurements also show that $\epsilon - 1$ at the end of the plasma is proportional to L .

Because the trap is not sufficiently long, the sectored ring cannot be used in the above-resonance regime.

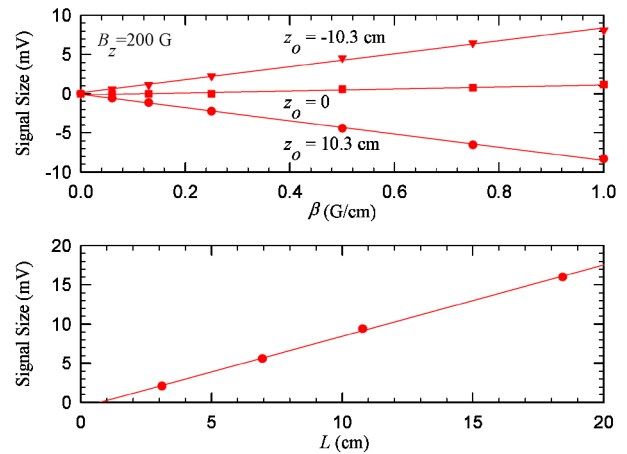


FIG. 3 (color online). A voltage signal, $(V_1 + V_3) - (V_2 + V_4)$, that is proportional to $\epsilon - 1$ shows that the below-resonance plasma has the shape of a magnetic flux tube.

However, the z -integrated plasma shape can be determined in all regimes by dumping the plasma onto the phosphor screen [16] and measuring the resultant light with a CCD camera. The CCD measurements in Fig. 4 show that the plasma changes from elliptical for $\omega t_T \ll 1$ (large B_z) to cylindrical for $\omega t_T \gg 1$ (small B_z), as expected.

As noted above, the quadrupole field induces radial excursions in the electron trajectories. In conjunction with electron-electron collisions, these excursions cause radial transport. We can measure the diffusion coefficient, D , from the time histories of the density profile $n(r, t)$ obtained from the CCD plasma images; i.e.,

$$D = \frac{dN/dt}{2\pi r dn/dr}, \quad (3)$$

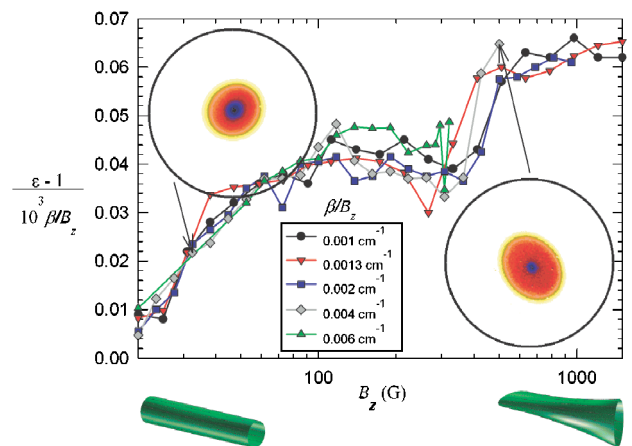


FIG. 4 (color online). The normalized ellipticity versus the axial field. The ellipticity increases as the axial field is increased and the plasma goes from above resonance to below resonance. Typical CCD plasma images are also shown, along with schematics of the inferred plasma shape.

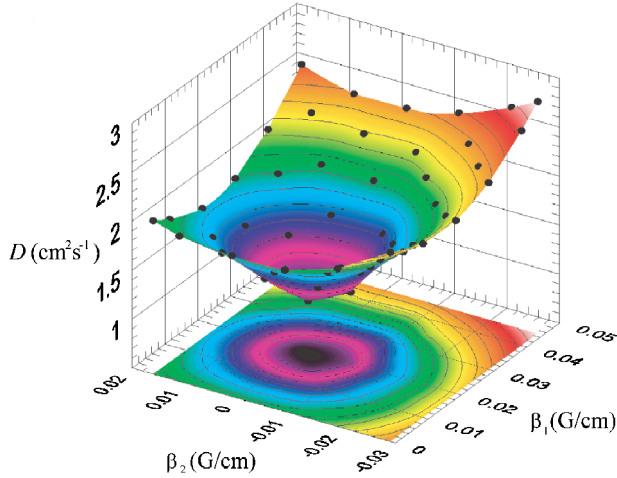


FIG. 5 (color online). Diffusion versus quadrupole field strength β_1 and β_2 , with $B_z = 100$ G, $r = 0.95$ cm, and $\omega = 2.0 \times 10^6$ rad s $^{-1}$. The data are represented by the solid dots.

where $N(t) = \int_0^r n(r', t) 2\pi r' dr'$. (We ignore the density's azimuthal dependencies because the quadrupole fields used for transport measurements are so small that the plasma is essentially cylindrical.) The shot-to-shot reproducibility of the system is so good that we can measure dN/dt by generating and holding plasmas for successively longer times; the density gradient dn/dr is measured from a single image. To compute $D(\omega)$, dn/dr and dN/dt are evaluated at fixed ω . A typical plot of D versus quadrupole strength is shown in Fig. 5. The minimum diffusion is offset from zero, implying that we correct for intrinsic field errors by applying a small quadrupole field.

To determine the dependence of D on the plasma rotation rate ω , we use measurements such as that shown in Fig. 5 to calculate the average value of D around a circle of radius 0.020 G/cm and centered on the minimum of $D(\beta_1, \beta_2)$. The statistical error in $D(\omega)$ is about 7%. Figure 6 shows $D(\omega)$ for several magnetic fields and densities, and fixed length $L = 28$ cm, radius $r = 0.95$ cm, and temperature $kT = 1.6$ eV [17]. The diffusion has a clearly visible resonance in ω once an overall scaling with B_z^{-2} is removed.

Although not shown here [18], the rotation frequency, ω_{peak} , where the peak diffusion occurs moves as expected for a bounce-resonance process when L and kT are varied. ω_{peak} moves to larger ω and the maximum value of the diffusion, D_{max} , decreases as L decreases. However, the exact dependence on L is difficult to determine. ω_{peak} moves to larger ω and D_{max} decreases as kT increases.

There are several other noteworthy features of the experimental data. First, over the available experimental range $\omega = 8.0 \times 10^5$ rad s $^{-1}$ to 3.0×10^6 rad s $^{-1}$, D scales like β^2 for $\beta \leq 0.020$ G/cm (see Fig. 7). This β^2 dependence is typical of transport in the so-called ‘‘plateau’’ regime [6]. Second, $D(\omega)$ scales like ω^2 at small ω ;

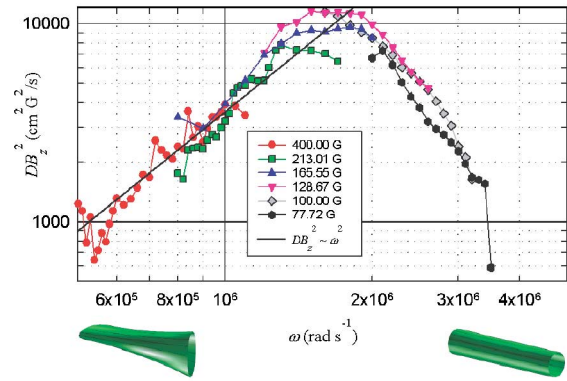


FIG. 6 (color online). The normalized diffusion, DB_z^2 versus the plasma rotation frequency ω . The rotation frequency is varied by changing both the magnetic field B_z and the plasma density; the field dependence is shown explicitly. For small ω the diffusion scales like ω^2 .

a least squares fit to the data with $\omega < 1.3 \times 10^6$ rad s $^{-1}$ in Fig. 6 gives an exponent of 2.05 ± 0.09 .

It is difficult to test the r dependence of D because the numerical noise in dn/dr becomes too great at both large and small radii where $dn/dr \sim 0$. Further, the numerical noise in dN/dt becomes too great at large radii.

In conclusion, we have applied an axially invariant, transverse quadrupole field to a pure electron plasma confined in a Malmberg-Penning trap. Whether the plasma is above or below resonance, ($\omega t_T \ll 1$ or $\omega t_T \gg 1$) determines the properties of both the plasma shape and the transport. Diffusion coefficients of order 1 cm 2 /s are observed at resonance for a perturbation of only 0.020 G/cm.

The ATHENA and ATRAP antihydrogen teams will have difficulty using quadrupole fields in conjunction with Malmberg-Penning traps. Typical experimental parameters for ATRAP will be $B_z = 2$ T, $n = 10^8$ cm $^{-3}$,

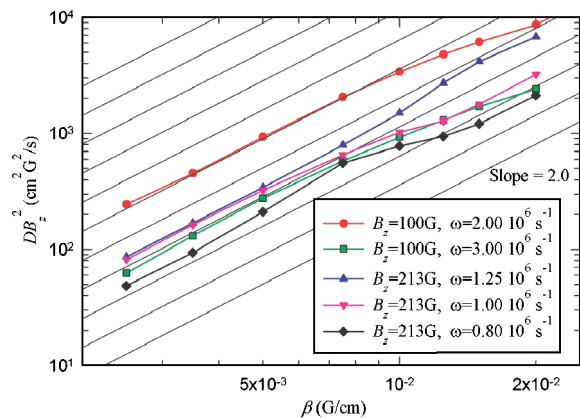


FIG. 7 (color online). The normalized diffusion as a function of the quadrupole strength β . Over a range of parameters, the diffusion scales like β^2 .

and $T = 4$ K [19]. We estimate that $\omega t_T \approx 0.6$, placing them near the resonance. Even if operating off resonance, the magnitude of the quadrupole field will be strong enough to severely limit confinement times. We note that our experiments contradict the conclusions of Ref. [20]. This reference, however, deliberately ignores the resonances that are key to this configuration.

Many of the results shown here can be predicted by a simple diffusive resonant particle transport calculation [21]. In this model, electrons take steps caused by the radial excursions described above, at a rate set by the plasma collision frequency. However, the simple theory predicts a resonant temperature that is too low by a factor of 4. A more detailed model, which would have to include a detailed calculation of the energy surfaces, and also the electron mobility, is beyond the scope of this Letter. Recently, Kabantsev [22] has proposed that these effects are related to trapped particle mode transport. This model may be able to explain the temperature discrepancy found in the resonant particle transport model, but its application to the quadrupole configuration is not straightforward.

This work was supported by the Office of Naval Research and by the Los Alamos National Laboratory.

*Present Address: Princeton Plasma Physics Laboratory.

Electronic address: egilson@pppl.gov

†Electronic address: joel@physics.berkeley.edu

- [1] R. Keinigs, Phys. Fluids **24**, 1447 (1981).
- [2] C. F. Driscoll and J. H. Malmberg, Phys. Rev. Lett. **50**, 167 (1983).
- [3] R. Keinigs, Phys. Fluids **27**, 206 (1984).
- [4] D. L. Eggleston and T. M. O'Neil, Phys. Plasmas **6**, 2699 (1999).
- [5] J. M. Kriesel and C. F. Driscoll, Phys. Rev. Lett. **85**, 2510 (2000).
- [6] D. D. Ryutov and G. V. Stupakov, Sov. J. Plasma Phys. **4**, 278 (1978).
- [7] D. D. Ryutov and G. V. Stupakov, Sov. Phys. Dokl. **23**, 412 (1978).
- [8] R. H. Cohen, Nucl. Fusion **19**, 1579 (1979).
- [9] R. H. Cohen, W. M. Nevins, and G. V. Stupakov, Nucl. Fusion **23**, 611 (1982).
- [10] B. V. Chirikov, Sov. J. Plasma Phys. **5**, 492 (1979).
- [11] M. H. Holzscheiter *et al.*, Hyperfine Interact. **109**, 1997 (1997).
- [12] G. Gabrielse and L. H. S. L. Rolston, Phys. Lett. A **129**, 38 (1988).
- [13] M. Amoretti *et al.*, Nature (London) **419**, 456 (2002).
- [14] When transport is present, the plasma's density and shape change with time. If the characteristic transport time is greater than the other time scales in the system, then the plasma exists in a slowly evolving quasiequilibrium state. It is the shape of this state that we measure.
- [15] Of course, the plasma ellipse must be aligned with the sectors; rotating the ellipticity by varying the quadrupole angle θ_o finds the appropriate $\cos(2\theta_o)$ dependence.
- [16] On dumping, the elliptical shape of the far end of a below-resonance plasma will rotate to orient itself properly relative to the near end shape. Above-resonance plasma images are more problematic as they will rotate and smear while dumping. However, the smearing is reduced by the electron acceleration during the dumping process. More importantly, exactly this same smearing explains why the plasma is round in the first place.
- [17] D. L. Eggleston, C. F. Driscoll, B. R. Beck, A. W. Hyatt, and T. H. Malmberg, Phys. Fluids B **4**, 3432 (1992).
- [18] E. P. Gilson, Ph.D. thesis, University of California, Berkeley, 2001.
- [19] G. Gabrielse (private communication).
- [20] T. M. Squires, P. Yesley, and G. Gabrielse, Phys. Rev. Lett. **86**, 5266 (2001).
- [21] E. Gilson and J. Fajans, in *Non-Neutral Plasma Physics IV*, edited by F. Andereg, L. Schweikhard, and C. Driscoll (American Institute of Physics, New York, 2002), p. 378.
- [22] A. A. Kabantsev and C. F. Driscoll, Phys. Rev. Lett. **89**, 245001 (2002).